Prediction of Interface Behavior of a Steel/CFRP Hybrid Part Manufactured by Stamping

Jae-Chang Ryu , Chan-Joo Lee , Do-Hoon Shin , Dae-Cheol Ko *

Posted Date: 24 July 2024

doi: 10.20944/preprints202407.1881.v1

Keywords: hybrid part; spring-back; stamping process; cohesive properties

 doi:10.20944/preprints202407.1881.v1

Article

Prediction of Interface Behavior of a Steel/CFRP Hybrid Part Manufactured by Stamping

Jae-Chang Ryu [1], Chan-Joo Lee [2], Do-Hoon Shin [3] and Dae-Cheol Ko [1,*]

[1] Department of Nanomechatronics Engineering, Pusan National University, Busan 46241, Republic of Korea
[2] Precision Manufacturing & Control R&D Group, Korea Institute of Industrial Technology, Jinju 52845, Republic of Korea
[3] Aerospace Engineering Team, Koreanair R&D Center, Busan 46712, Republic of Korea
* Correspondence: dcko@pusan.ac.kr; Tel.: +82-51-510-3697

Abstract: Carbon fiber reinforced plastic (CFRP) is one of the representative lightweight material. The automotive industry has focused on producing the steel/CFRP hybrid part to reduce the weight. After manufacturing, delamination can occur at the interface between the CFRP and steel owing to the hybrid part constituting dissimilar materials. However, most studies have focused only on designing the manufacturing processes for hybrid part or evaluating the adhesive used at the interface. Therefore, it is necessary to predict the behavior of the interface after demolding the hybrid part. This study aimed to predict the interface behavior of a steel/CFRP hybrid part by considering its forming and cohesive properties. First, double cantilever beam (DCB) and end-notched flexure (ENF) tests were performed to obtain cohesive parameters, such as energy release rate of modes Ⅰ and Ⅱ ($G_{Ⅰ}$, $G_{Ⅱ}$). The experimentally obtained properties were applied to the bonding area of the hybrid part. Subsequently, a forming simulation was performed to obtain the stress of the steel blank in the hybrid part. The stress distribution after forming was utilized as the initial condition for spring-back simulation. Finally, the interface behavior of the hybrid part was predicted by a spring-back simulation, and the results were compared with the experimental results for verification.

Keywords: hybrid part; spring-back; stamping process; cohesive properties

1. Introduction

Recently, there has been an increased effort to study different ways to improve fuel efficiency and overcome environmental pollution in the automotive industry. One of the effective solutions to improve fuel efficiency is making the vehicle lightweight. Carbon fiber reinforced plastic (CFRP) is a lightweight material with higher specific strength and stiffness than steel materials. Therefore, many studies have been conducted on the application of CFRP materials in automotive parts [1–3].

Steel/CFRP hybrid part has been investigated in various studies because of their several advantages, including high strength and lightweight. Qihua et al. investigated the transverse crashworthiness characteristics of a steel/CFRP tube manufactured using filament winding [4]. They discussed the effects of the winding sequence, number of layers, and bending collapse behavior on the plastic deformation of the hybrid part using bending tests. Consequently, a modified theoretical model for bending prediction was proposed for the elastic and plastic regions. However, the proposed model was limited to hybrid tubes. Kim et al. designed a hybrid B-pillar to improve crashworthiness through design optimization and impact analysis [5]. In addition, they produced a hybrid part by assembling a composite reinforcement and steel outer with an adhesive. Drop-tower tests of the conventional and hybrid parts were conducted, and it was confirmed that the crashworthiness of the hybrid B-pillar improved, as expected in the simulation. However, the manufacturing process employed was not economical because of the necessity of the assemble

 doi:10.20944/preprints202407.1881.v1

process for the manufactured parts. Taylor et al. manufactured a hybrid part using a one-step process, which was compared with a traditional manufacturing process [6]. Hybrid parts fabricated through a one-step process with economic advantages indicated slightly lower flexural stiffness and strength but higher strain to failure and higher energy absorption. Kim et al. designed manufacturing processes using finite element (FE) simulations and manufactured a steel/CFRP hybrid part using prepreg compression molding (PCM) [7]. The hybrid part was produced by forming a CFRP reinforcement on a hot-stamped B-pillar to eliminate the additional assembly process. However, their manufacturing process comprised two stages because it involved forming a steel outer and forming CFRP on the preformed steel outer. Lee et al. manufactured a steel/CFRP hybrid part without preformed components [8]. A hybrid blank composed of a CFRP prepreg and steel sheet was employed to reduce the number of manufacturing processes. An FE simulation was conducted to investigate the contact pressure during the manufacturing process. The mechanical properties of the part deteriorated in the regions with low contact pressures. However, they did not discuss potential problem such as delamination of the interface between the CFRP and steel.

In the manufacturing of steel/CFRP hybrid part, delamination at the interface can occur because of the different material behaviors. During the manufacturing of the CFRP part, spring-in, which is the opposite deformation to the spring-back of the steel part, occurs when the formed part is demolded from the molds [9,10]. Therefore, predicting the interface behavior between the steel and CFRP is necessary. Yuyang et al. introduced a bond-slip model of the steel/CFRP interface and investigated the effects of the adhesive type, adhesive thickness, and CFRP type on the interface behavior using the 3D-DIC method [11]. They reported that the adhesive thickness and inter-laminar shear properties of the CFRP plate significantly affected the bond-slip model, and verified the results through a comparison with experimental results. Abderrahim et al. investigated the behavior of a steel tube strengthened by a composite using the cohesive zone model (CZM), a well-known finite element model (FEM) for predicting adhesive behavior [12]. They presented numerical and experimental results for 15 specimens with different composite thicknesses, and steel tube thicknesses and lengths. Zhen et al. developed a CZM with a user subroutine (UMAT) for the hybrid part [13]. A simulation of the single-lap test using the proposed method was performed, and the results were compared with the experimental results. Minnicino et al. performed an FE simulation of a microdroplet test to consider the progressive damage of the interphase using surface-based cohesive behavior, where the contact behavior theory is identical to the cohesive element used in the ABAQUS software [14]. In addition, they investigated the influence of various geometric parameters, such as blade opening, fiber-free length, and fiber diameter, on cohesive damage. However, most of these studies did not consider forming process of the hybrid part and focused on simple geometries. Hwang et al. investigated the effects of surface treatment on the bonding strength and spring-back of a CR980/CFRP hybrid part [15]. The increased bonding strength was dependent on the degree of surface treatment. Moreover, the spring-back angle of the hybrid part increased with the surface roughness. However, their study did not consider the interface behavior in the hybrid part. Park et al. predicted the interface behavior of a steel/CFRP hybrid part manufactured by stamping [16]. Double cantilever beam (DCB) and end-notched flexure (ENF) tests were conducted to obtain the energy release rate of the mixed mode, which was applied to the FE simulation using the CZM. However, they employed a displacement equal to the amount of spring-back experimentally measured as a boundary condition. In other words, their method was not suitable for applications involving complicated geometries.

This study aims to predict the interface behavior of steel/CFRP hybrid part manufactured by stamping. First, DCB and ENF tests were performed to obtain the cohesive properties, such as the energy release rate of modes I and II. The properties obtained from the DCB and ENF tests were applied to the interface between the CFRP and steel. Second, a forming simulation of the steel/CFRP hybrid part was performed to obtain the residual stress in the steel part. The stress distribution of the steel obtained from forming simulation was used as a boundary condition to predict the delamination at the interface of the hybrid part during the spring-back simulation. Finally, a hat-shaped hybrid part was manufactured through stamping and compared with the FE results for verification.

 doi:10.20944/preprints202407.1881.v1

2. Materials and Methods

2.1. Stamping Process for Manufacturing the Steel/CFRP Hybrid Part

In this study, a stamping process was employed to manufacture steel/CFRP hybrid part. The CFRP reinforcement and steel outer were formed and assembled in a single step to reduce the number of manufacturing processes by the remove of additional assemble process [17]. Figure 1 shows the entire manufacturing process of the steel/CFRP hybrid part: (a) transferring the blank consisting of the CFRP patch and steel sheet to the lower die; (b) descending the punch to deform the blank, which is held by a pad and holders; (c) curing the formed part in the closed tool set; (d) demolding the hybrid part from the tool set, consisting of a punch, blank holder, lower die, and pad.

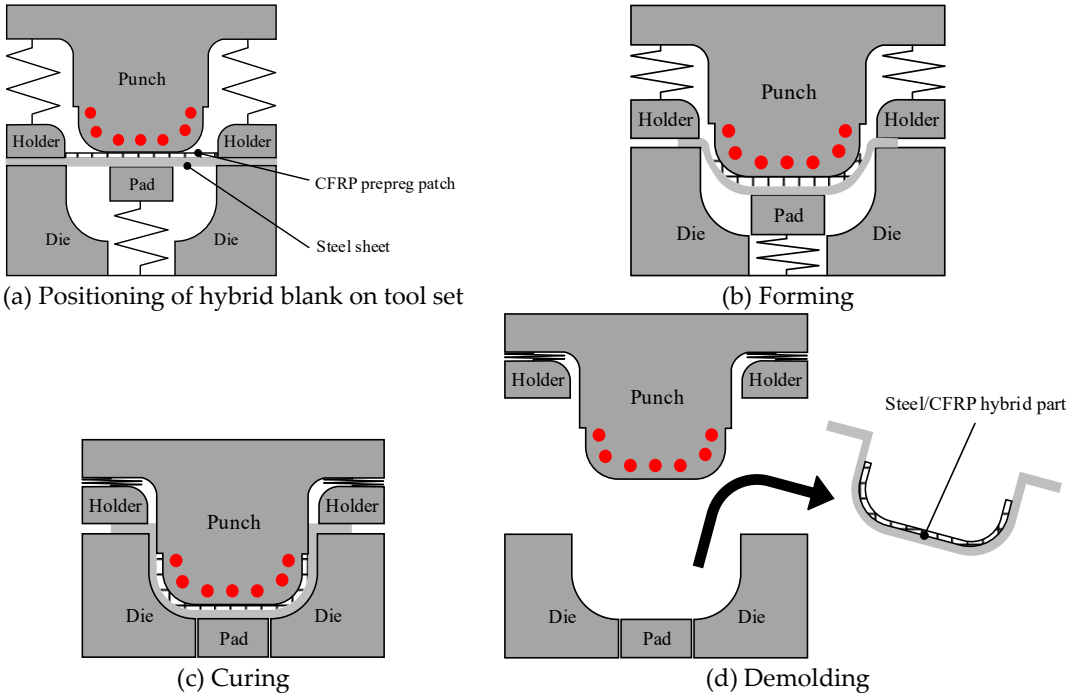

Figure 1. Manufacturing process of the steel/CFRP hybrid part [17].

Generally, the deformation during the ejection of the formed composite part is spring-in, while that at the ejection of the formed steel part is spring-back, which occurs in the opposite direction. Therefore, delamination can occur at the interface of hybrid part after manufacturing. However, many of the studies mentioned in Section 1 focused only on the forming of a hybrid part or the properties of the adhesive. They did not consider potential problem after manufacturing, such as delamination in the bonding area. Figure 2 illustrates the procedure of the FE simulation employed in this study for predicting the delamination of the steel/CFRP hybrid part. First, the DCB and ENF tests were conducted to obtain the cohesive properties in the normal and shear directions. Second, a forming simulation was performed considering manufacturing conditions, to obtain the stress distribution of the steel material after stamping. Finally, the interface behavior of the hybrid part was predicted using a spring-back simulation. Here, the stress obtained from forming simulation was used as the initial condition. Additionally, the cohesive properties obtained from the DCB and ENF tests were applied to the bonding area of the hybrid part.

 doi:10.20944/preprints202407.1881.v1

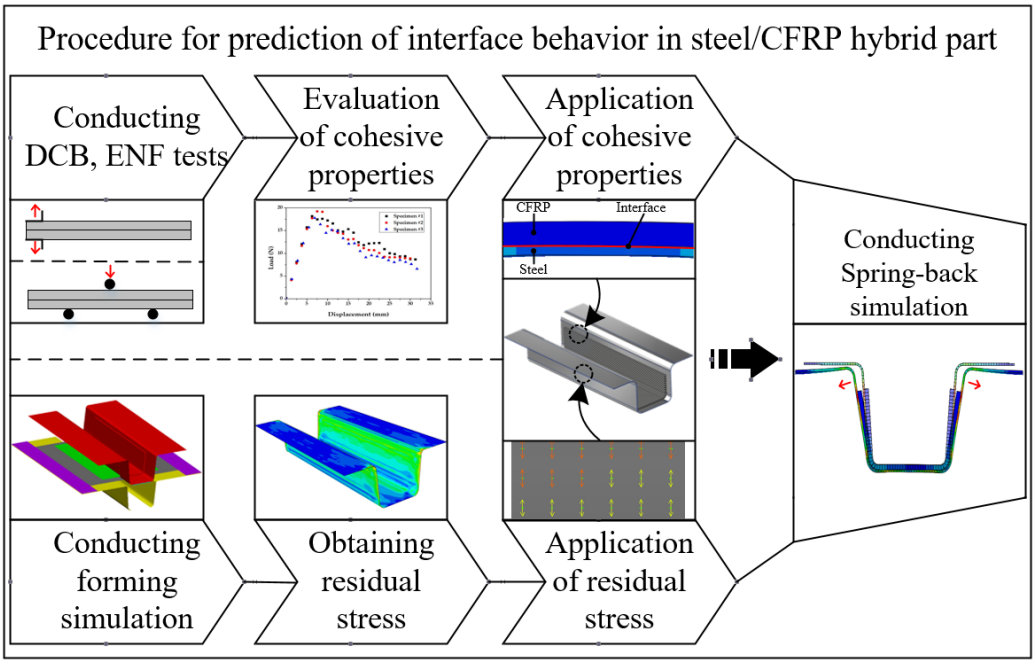

Figure 2. Procedure of FE simulation for prediction of interface behavior of the hybrid part.

2.2. Evaluation of the Cohesive Properties at the Bonding Area

In general, the delamination in the bonding area occurred in the normal (mode I) and shear directions (mode II). In this study, DCB and ENF tests were performed to obtain the cohesive properties of the bonding area. The specimens were fabricated using a DP590 sheet (Hyundai Steel, Dangjin, South Korea) and CFRP (SK Chemicals, Seongnam, South Korea). The CFRP was a twill-weave prepreg and stocked in the 0° fiber direction. The specimens were cured for 3 min at 160℃ under the curing condition of the fast-cured epoxy. The release film was inserted between the steel plate and CFRP to create the initial crack for each test.

A DCB test was performed to evaluate the cohesive properties of mode I. The specimens were fabricated according to ASTM 5528-13 [18]. Tests were conducted using an INSTRON universal testing machine (INSTRON 5566A; Instron, Norwood, MA, USA). The velocity of the upper jig was 5 mm/min, while the lower jig held the lower hinge to restrict the vertical movement, as shown in Figure 3. The energy release rate of mode Ⅰ (G_I) is calculated by the modified beam theory (MBT), which is given by

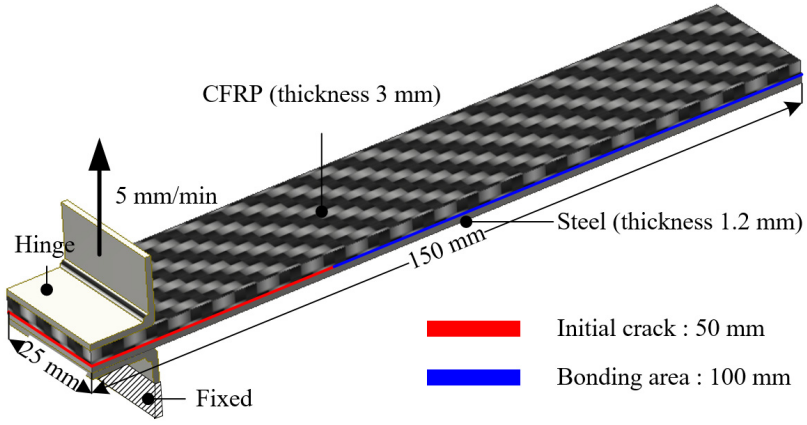

Figure 3. Dimension of specimen for DCB test.

Preprints.org (www.preprints.org) | NOT PEER-REVIEWED | Posted: 24 July 2024 doi:10.20944/preprints202407.1881.v1

$$G_I = \frac{3P_t\delta_t}{2B(a_0+|\Delta|)} \quad (1)$$

where P_t, δ_t, B, and a_0 are the maximum load, the displacement of the upper jig corresponding to the load, the specimen width, and the length of the separation, respectively. Δ is calculated by plotting the least squares of the cube root of compliance ($C^{1/3}$) with respect to the delamination length [16].

An ENF test was conducted to evaluate the cohesive properties of mode II. The specimens were fabricated for the experiments according to the ASTM D7905 standard [19]. The punch, at a velocity of 2 mm/min, descents to the specimen supported by the supporters, as shown in Figure 4. The energy release rate of mode II (G_{II}) is expressed as

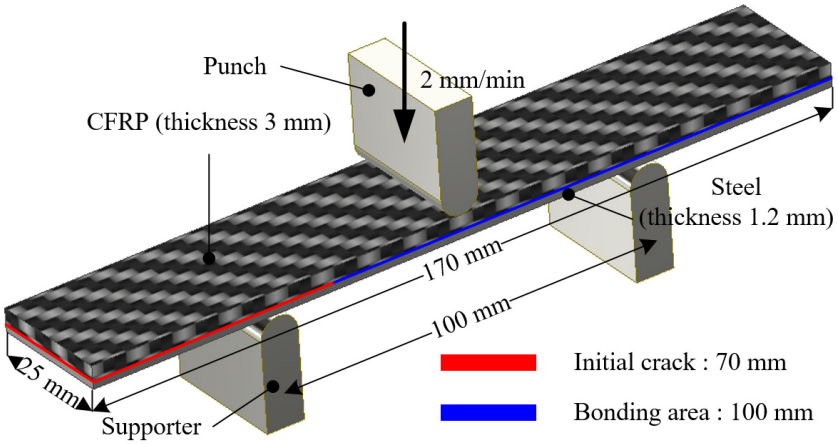

Figure 4. Dimension of specimen for ENF test.

$$G_{II} = \frac{9a_0^2P_c\delta_c}{2B(2L^3+3a_0^3)} \quad (2)$$

where a_0, P_c, δ_c, B, and L are the crack length, load corresponding crack occurrence, displacement of punch at the crack occurrence, width of specimen, and distance between both supporters.

2.3. Verification of Cohesive Properties by FE Simulation

In this study, FE simulations of the DCB and ENF tests were performed using the commercial FE software ABAQUS 2020 to verify the obtained cohesive properties. In the FE simulation, the energy release rate along the direction is an essential input parameter. Table 1 lists the mechanical properties of the CFRP and the energy release rates of modes I and II. The FE model and boundary conditions for each test are shown in Figure 5. The steel and CFRP were modeled using a 4-node rectangular shell mesh. In addition, the CFRP layup and steel thickness were applied to the element. In the DCB test, vertical displacement (U_Z) was applied to the upper hinge. Fixed conditions except for the axial rotation (R_X) of the hinge were applied to describe the rotational freedom of the hinge in the experiment, as shown in Figure 5 (a). The vertical displacement (U_Z) of the punch and the fixed conditions of the supporters were employed in the FE model, similar to the actual ENF test, as illustrated in Figure 5 (b).

Table 1. Material properties of CFRP and bonding area used in FE simulation.

	Property	Value
CFRP	Elastic modulus in 0° direction	65.01 GPa
	Elastic modulus in 90° direction	65.01 GPa
	Shear modulus in 1-2 plane	12.69 GPa
	Shear modulus in 2-3 plane	1.38 GPa
	Shear modulus in 1-3 plane	1.38 GPa

 doi:10.20944/preprints202407.1881.v1

	Poisson's ratio	0.13
Bonding area	Energy release rate of mode Ⅰ	0.13 N/mm
	Energy release rate of mode Ⅱ	4.96 N/mm

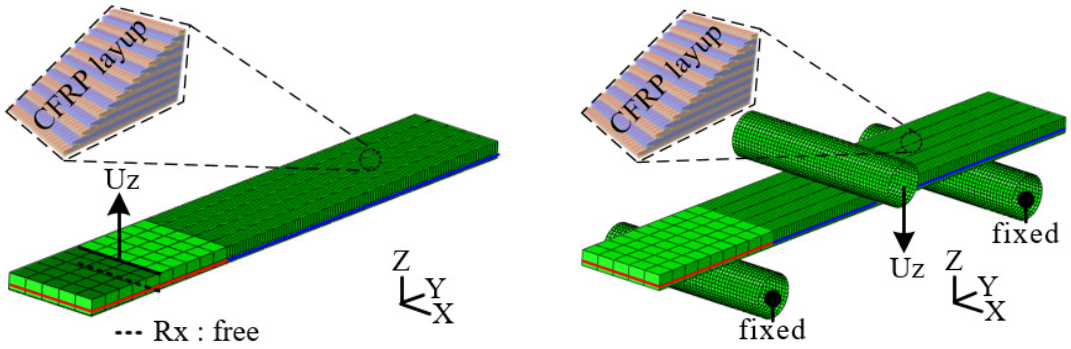

Figure 5. FE model and boundary conditions of experiments: (a) DCB test; (b) ENF test.

Figure 6 presents the results of the FE simulation compared with the experimental results of the DCB and ENF tests. The FE simulation using the cohesive properties of modes I and II was in good agreement with the experimental results in the load-displacement curve. The cohesive properties, verified by a comparison of the FE simulation and experiments were employed to predict the interface behavior of the hybrid part in Section 3.

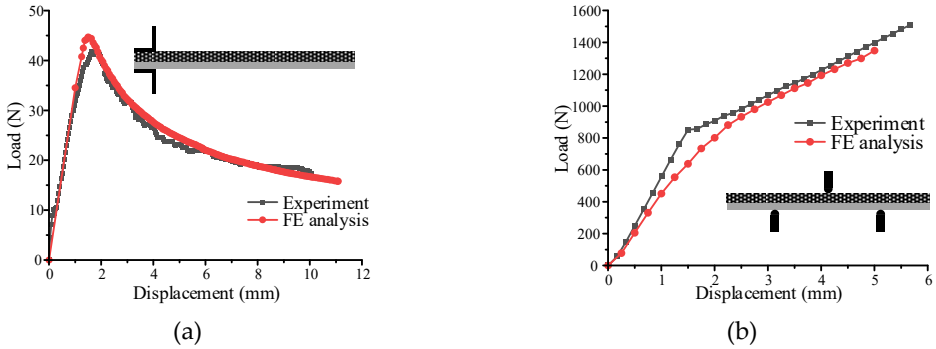

Figure 6. Comparison of FE simulation and experiments: (a) DCB test; (b) ENF test.

3. Prediction of the Interface Behavior of the Steel/CFRP Hybrid Part by Stamping

3.1. Forming Simulation of the Steel/CFRP Hybrid Part

In this study, an FE simulation of the stamping process was performed considering the manufacturing conditions using the commercial FE software PAM-FORM 2020. Figure 7 shows the FE model of the stamping process, which was divided into the initial state, holding, and forming. In the initial state, a hybrid blank composed of a thermoset CFRP prepreg and a steel sheet was placed on the tool set, as shown in Figure 7 (a). Two types of steel sheets, DP590 and DP780, were utilized to investigate the effect of residual stress on delamination. Table 2 summarizes the mechanical properties of DP590 and DP780. Reference data to consider forming of prepregs were applied to the shear deformation properties of the CFRP [17]. In the FE model, the CFRP and steel were modeled using a 4-node rectangular shell element. The mesh sizes of the CFRP and steel were 2 and 4 mm, respectively. The thicknesses of the CFRP and steel were 3 and 1.2 mm, respectively. Holder and pad force of 11 kN and 13 kN were applied to hold the blank, as shown in Figure 7 (b). The velocity of the punch was 10 mm/s, and the die was fixed, as shown in Figure 7 (c). The stress distribution in the

 doi:10.20944/preprints202407.1881.v1

steel material during stamping was obtained from the simulation and then used as the initial condition in the spring-back simulation.

Table 2. Mechanical properties of DP590 and DP780.

	DP590	DP780
Elastic modulus	210 GPa	
Yield strength	390 MPa	527 MPa
Tensile strength	679 MPa	957 MPa
Blank thickness	1.2 mm	

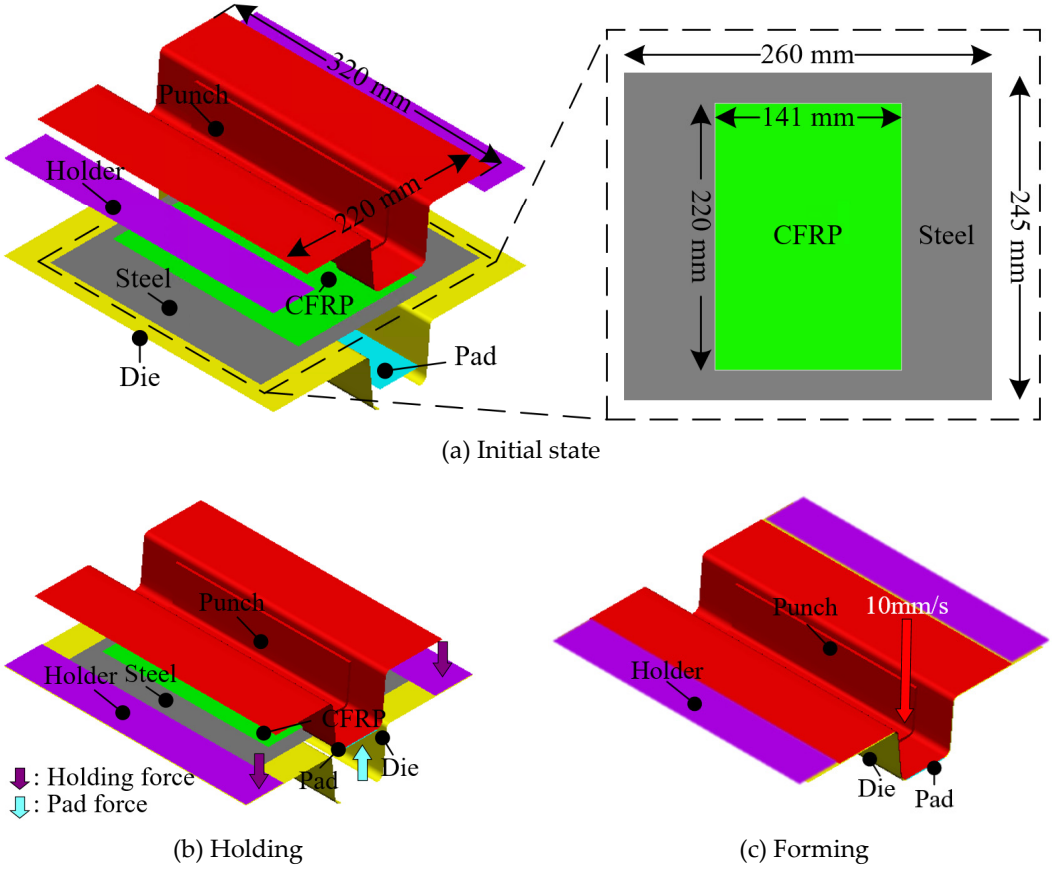

Figure 7. FE model of the stamping process for manufacturing the steel/CFRP hybrid part.

3.2. Spring-Back Simulation of the Hybrid Part

As mentioned in Section 2.1, deformations after stamping the CFRP and steel parts occurred in opposite directions. However, most studies on hybrid part have focused only on forming or interface behavior. They did not consider other potential problem, such as delamination after stamping. Therefore, the prediction of the interface behavior after manufacturing is important.

In this study, the interface behavior of the hybrid part was predicted using the results of forming and cohesive properties. First, the deformed shapes from the forming simulation were employed to predict delamination. The stress distribution of the steel part in PAM-FORM was transferred to ABAQUS using the user subroutine SIGINI, allowing users to define the initial stress in the model before the simulation. Cohesive properties were also applied at the interface of the hybrid part. Figure 8 shows the boundary conditions for the spring-back simulations. A fully fixed (translations and rotations in X, Y, and Z directions) constraint at the center point and two restricted points (translation

 doi:10.20944/preprints202407.1881.v1

in the Z direction for one, and translations in Y and Z directions for the other) were applied to prevent rigid body modes.

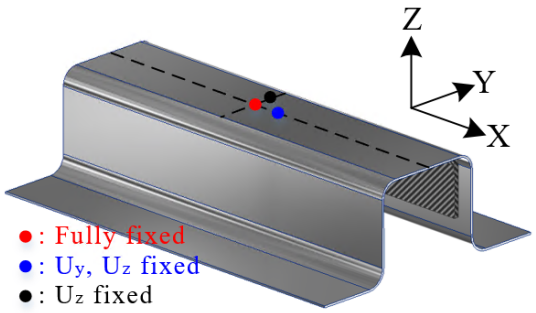

Figure 8. Boundary conditions for the spring-back simulation.

Figure 9 shows the initial states of the spring-back simulation. The stress distributions of DP590 and DP780 were used to perform spring-back simulations of DP590/CFRP and DP780/CFRP. The stress in the bottom area was lower than ones in other areas because the punch and pad held it from the beginning to the end of the forming process, resulting in minimal deformation. However, the stress at the wall was higher than ones at the bottom because various deformations, such as bending and tension, occurred during the forming process, as shown in Figure 7. Subsequently, a spring-back simulation was conducted to predict the interface behavior. Table 1 lists the cohesive properties applied to the bonding area. Although the experiments were performed using only DP590 steel, this was acceptable for DP780/CFRP because the DCB and ENF tests were performed within the elastic deformation region of the adherend. Figure 10 presents the damage of interface after spring-back simulations. The damage value progresses from 0 to 1. When the value of damage reaches to 1, it means the delamination occurs at the interface. The FE simulation predicted that delamination would not occur in the DP590/CFRP hybrid part, as shown in Figure 10 (a). However, for DP780/CFRP, debonding was predicted to occur at the wall of the hybrid part, as shown in Figure 10 (b). Compared to the wall, CFRP and steel were attached to the bottom of the hybrid part. Generally, the amount of spring-back increased with the increase in the strength of steel material. Figure 11 shows the shapes of initial state and after spring-back in the middle section of the hybrid part. The steel outers moved outside, and the deformation value of DP780 was higher than that of DP590, as shown in view A.

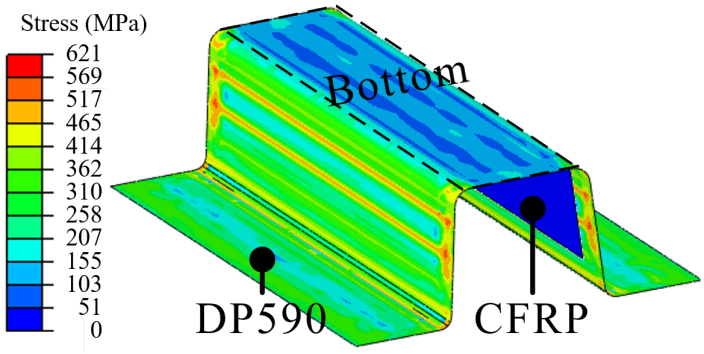

(a)

 doi:10.20944/preprints202407.1881.v1

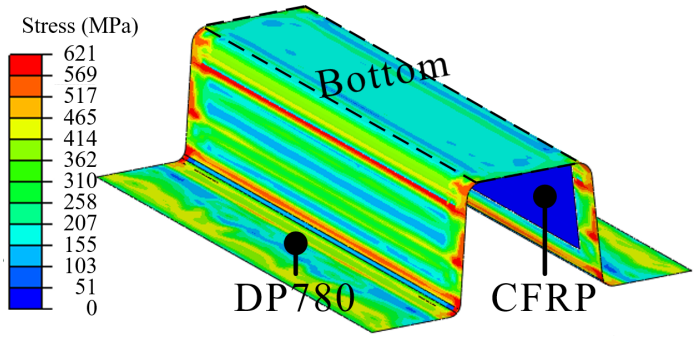

(b)

Figure 9. Stress distribution used as initial state: (a) DP590; (b) DP780.

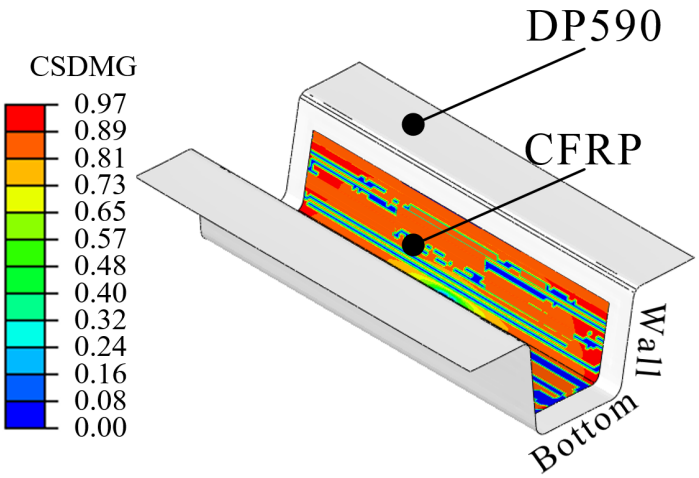

(a) DP590/CFRP

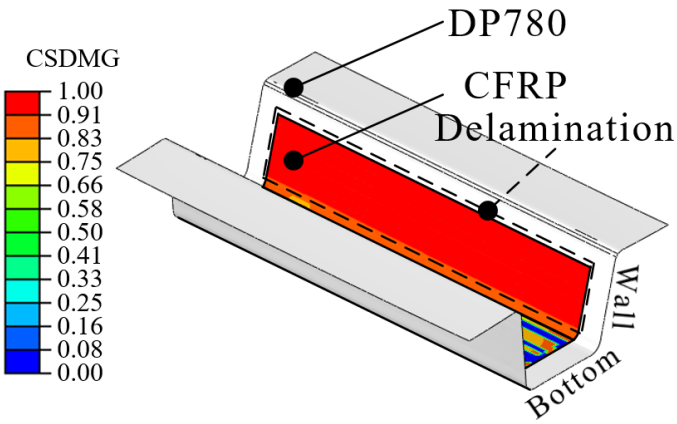

(b) DP780/CFRP

Figure 10. FE results of spring-back simulation.

 doi:10.20944/preprints202407.1881.v1

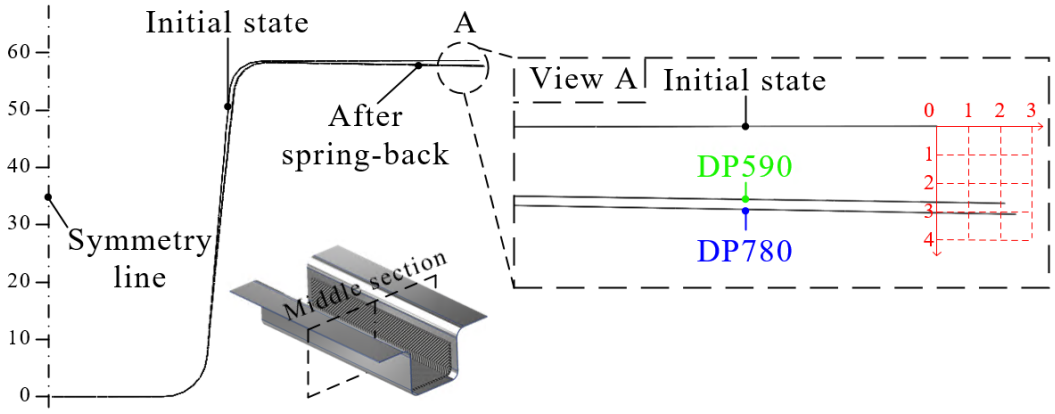

Figure 11. Comparison of initial state and spring-back state.

4. Experimental Verifications

In this study, steel/CFRP hybrid parts were manufactured to validate FE simulation results. The experimental cases were classified as DP590/CFRP and DP780/CFRP. Figure 12 illustrates the equipment used to produce hybrid parts through stamping. The tool set consisted of a punch with an inserted cartridge heater, blank holders, a lower die, and a pad placed on a 2000-kN servo press. The punch was preheated to 160℃ considering the curing condition of CFRP material. The hybrid blank was composed of steel and CFRP and placed on the die.

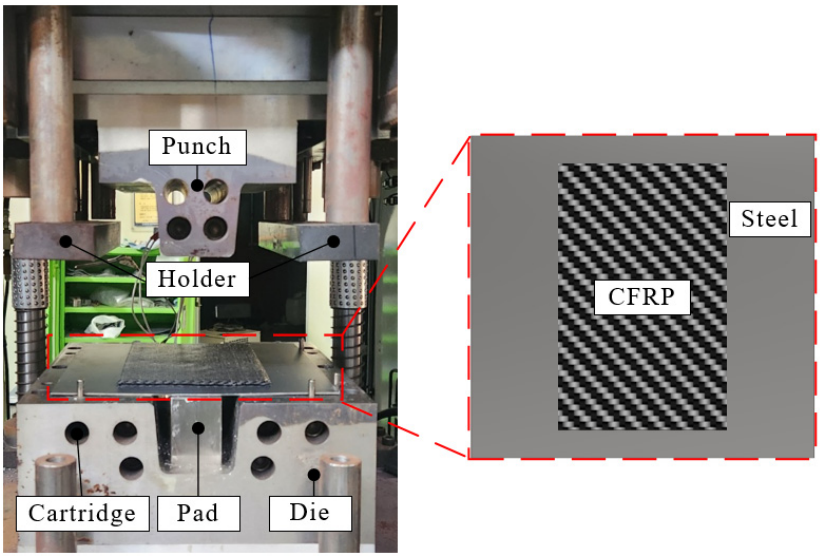

Figure 12. Experimental equipment to manufacture the steel/CFRP hybrid part.

The manufacturing process of the steel/CFRP hybrid part is as follows. First, the liquid release agent was spread on the surfaces of the tool set to prevent CFRP from sticking to the molds. Subsequently, the preheated punch is moved down to form a blank held by the blank holders and pad. After forming, the hybrid part was cured within closed molds. Finally, the hybrid component was ejected after curing for 3 min.

The experimental and FE simulation results were compared to verify the results predicted by the FE simulation. Figure 13 presents the experimental results obtained using DP590/CFRP and DP780/CFRP. In the DP590/CFRP hybrid part, steel and CFRP were attached to all the bonding areas, whereas delamination occurred at the interface in the DP780/CFRP hybrid part. The wall of the hybrid part was separated, as predicted by FE simulation in Figure 10 (b). However, some discrepancies were noted at the bottom surface, where partial delamination was observed

 doi:10.20944/preprints202407.1881.v1

experimentally, unlike the simulation results. Corner at the bottom, near the wall, was separated in the experiment, as shown in Figure 13 (b). In the simulation, the bottom remained bonded, whereas slight delamination occurred at the bottom in the experiment, as shown in Figures 10 (b) and 13 (b). The result of verification indicated that the additional consideration is required when using higher strength steels to prevent delamination. The prediction method of this study can be developed by investigating thermomechanical influences during curing and cooling on the interface behavior. The steel part is heated during curing and cooled after ejection. Therefore, the steel part shrink after being ejected from the toolset. However, the shrinkage of the thermoset composite is considerably small compared to that of steel. This indicates that the damage in the bonding area can progress due to the shrinkage of the outer steel. The accuracy of the spring-back simulation can be improved by investigating the thermal effects of delamination. These findings indicate the feasibility of the coupled analysis of forming simulation with cohesive properties for predicting interface behavior, although improvements are needed for greater accuracy, particularly in the DP780/CFRP case.

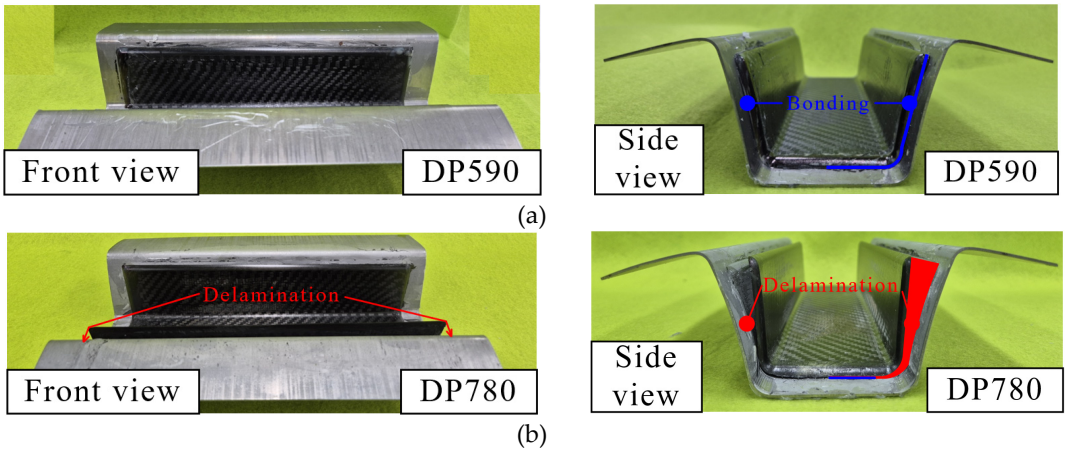

Figure 13. Hybrid part: (a) DP590/CFRP; (b) DP780/CFRP.

The proposed method can contribute to reduce the cost for producing hybrid part prior to actual manufacturing. If the manufacturing process is established, a coupled analysis can be utilized to predict the occurrence of delamination in the hybrid part. If the adhesive is predetermined, the analysis can be used to prevent delamination by optimizing the forming process parameters. The study enhances the reliability and quality of the parts by predicting delamination through the coupled analysis. This ensures better performance and lower defect rates in the final products.

In addition, this method can be used for ultralightweight hybrid part consists of other lightweight material such as aluminum. Generally, the amount of spring-back of aluminum part is greater than that of steel one due to the difference of mechanical properties. Therefore, the application of aluminum outer for hybrid part is more challenging compared to steel outer. The proposed method can be used to predict the occurrence of delamination and optimize the forming process to accommodate the higher spring-back of aluminum, thereby facilitating the use of aluminum in ultralightweight hybrid part. This makes it possible to take the benefits of aluminum's low weight while maintaining structural performance.

5. Conclusion

In this study, the interface behavior of a steel/CFRP hybrid part manufactured by stamping was predicted via FE simulation and verified through the comparison with experimental results. The results of the FE simulation were as follows. First, the DCB and ENF tests were performed to evaluate the cohesive properties of modes I and II. Cohesive properties were applied to describe the interface behavior of the hybrid part. Second, a forming simulation was performed considering actual manufacturing conditions. A hybrid blank consisting of a CFRP patch and a steel sheet was employed for one-step forming. In the final step of the proposed method, a spring-back simulation was

 doi:10.20944/preprints202407.1881.v1

performed using the stress distribution of steel part and the obtained cohesive properties. Here, the stress distribution of the steel material at the end of forming was employed as the initial state from PAM-FORM to ABAQUS using the user subroutine SIGINI code. In addition, cohesive properties were applied to the bonding area to predict the interface behavior after ejecting the hybrid part. The FE simulation cases were classified as DP590/CFRP or DP780/CFRP. Consequently, the FE simulation of DP590/CFRP predicted that delamination would not occur. However, the FE results of the DP780/CFRP showed delamination at the sidewall of the hybrid part. Hybrid parts were manufactured using DP590/CFRP and DP780/CFRP to verify the FE approach. A comparison of both cases indicated that the proposed FE approach was reasonable and in good agreement. Therefore, the FE simulation performed in this study is appropriate for predicting the interface behavior of hybrid part manufactured via stamping.

Author Contributions: Conceptualization, D.-C.K.; methodology, D.-H.S. and D.-C.K.; software, J.-C.R.; validation, C.-J.L., D.-H.S. and D.-C.K.; formal analysis, J.-C.R. and D.-C.K.; investigation, C.-J.L. and D.-H.S.; resources, C.-J.L.; data curation, J.-C.R.; writing—original draft preparation, J.-C.R.; writing—review and editing, D.-C.K.; visualization, D.-C.K.; supervision, D.-C.K.; project administration, D.-C.K.; funding acquisition, D.-C.K. All authors have read and agreed to the published version of the manuscript.

Funding: This research was funded by the National Research Foundation of Korea [2021R1I1A3A04037420]; Ministry of Trade, Industry & Energy [No. 20007444].

Institutional Review Board Statement: Not applicable.

Informed Consent Statement: Not applicable.

Data Availability Statement: The data presented in this study are available on request from the corresponding author and the first author and the first author on reasonable request.

Conflicts of Interest: The authors declare no conflicts of interest.

References

1. Pan, F.; Zhu, P.; Zhang, Y. MetaModel-based lightweight design of B-pillar with TWB structure via support vector regression. Comput. Struct. 2010, 88, 36-44.
2. Liu, Q.; Lin, Y.; Zong, Z.; Sun, G.; Li, Q. Lightweight design of carbon twill weave fabric composite body structure for electric vehicle. Compos. Struct. 2013, 97, 231-238.
3. Kim, K.S.; Bae, S.Y.; Oh, S.Y.; Seo, M.K.; Kang, C.G.; Park, S.J. Trend of carbon fiber reinforced composites for lightweight vehicles. Elastom. Compos. 2012, 47, 65-74.
4. Qihua, Ma.; Jiarui, Sun.; Xuehui, Gan.; Zeyu, Sun. Experiment and modified model for CFRP/steel hybrid tubes under quasi-static transverse loading. International journal of crashworthiness. 2021, 26(3), 343-353.
5. Kim, D.J.; Lim, J.Y.; Nam, B.G.; Kim, H.J.; Kim, H.S. Design and manufacture of automotive hybrid Steel/Carbon Fiber composite b-pillar component with high crashworthiness. International journal of precision engineering and manufacturing-green technology. 2020, 8, 547-559.
6. Tom, Taylor.; David, Penney.; Jun, Yanagimoto. One-step process for press hardened Steel-Carbon Fiber Reinforced Thermoset Polymer hybrid parts. Steel research international. 2020, 91, 2000085-8000093.
7. Kim, J.H.; Jung, Y.H.; Lambiase, Francesco.; Moon, Y.H.; Ko, D.C. Novel approach toward the forming process of CFRP reinforcement with a hot stamped part by prepreg compression molding. Materials. 2022, 15, 4743-4756.
8. Lee, M.S.; Kang, C.G. Determination of forming procedure by numerical analysis and investigation of mechanical properties of steel/CFRP hybrid composites with complicated shapes. Composite Structures. 2017, 164, 118-129.
9. Bellini, C.; Sorrentino, L.; Polini, W.; Corrado, A. A spring-in analysis of CFRP thin laminates: Numerical and experimental results. Composite Structures. 2017, 179, 17-24.
10. Groh, F.; Kappel, E.; H?hne, C.; Brymerski, W. Investigation of fast curing epoxy resins regarding process induced distortions of fibre reinforced composites. Composite structures. 2019, 207, 923-934.
11. Yuyang, Pang.; Gang, Wu.; Haitao, Wang.; Danying, Gao.; Pu, Zhang. Bond-slip model of the CFRP-steel interface with the CFRP delamination failure. Composite structures. 2021, 256, 113015-113027.
12. Abderrahim, Djerrad.; Feng, Fan.; Xudong, Zhi.; Qijian, Wu. Experimental and FEM analysis of AFRP strengthened short and long steel tube under axial compression. Thin-Walled Structures. 2019, 139, 9-23.
13. Zhen, Wang.; Guijun, Xian. Cohesive zone model prediction of debonding failure in CFRP-to-steel bonded interface with a ductile adhesive. Composites science and technology. 2022, 230, 109315-109323.

 doi:10.20944/preprints202407.1881.v1

14. Michael, Minnicino.; Michael, Santare. Modeling the progressive damage of the microdroplet test using contact surfaces with cohesive behavior. Composites Science and Technology. 2012, 72, 2024-2031.
15. Hwang, J.H.; Jin, C.K.; Lee, M.S.; Choi, S.W.; Kang, C.G. Effect of surface roughness on the bonding strength and spring-back of a CFRP/CR980 hybrid composite. Materials. 2018, 8, 715-726.
16. Park, J.S.; Kim, J.H.; Park, J.H.; Ko, D.C. Prediction of the delamination at the steel and CFRP interface of hybrid composite part. Materials. 2021, 14, 6285-6296.
17. Ryu, J.C.; Kim, J.H.; Kam, D.H.; Ko, D.C. Feasibility of one-shot forming for manufacturing of steel/CFRP hybrid b-pillar. Materials and Manufacturing Processes. 2022, 37(14), 1664-1678.
18. ASTM D5528-13. Standard test method for Mode Ⅰ interlaminar fracture toughness of unidirectional fiber-reinforced polymer matrix composites; ASTM international: West Conshohocken, PA, USA, 2013.
19. ASTM D7905. Standard test method for determination of the Mode Ⅱ interlaminar fracture toughness of unidirectional fiber-reinforced polymer matrix composites; ASTM international: West Conshohocken, PA, USA, 2014.